Active Suspension Design Requirements for Compliant Boundary Condition Road Disturbances

Anirudh Srinivasan

Thesis submitted to the faculty of the Virginia Polytechnic Institute and State University in partial fulfillment of the requirements for the degree of

Master of Science

In

Mechanical Engineering

Steve C. Southward, Chair

Diana Bairaktarova

Corina Sandu

27th July, 2017

Blacksburg, VA

Keywords: Active Suspension, Compliant Road, LMS adaptation, Actuator, Control Force

Active Suspension Design Requirements for Compliant Boundary Condition Road Disturbances

Anirudh Srinivasan

ABSTRACT

The aim of suspension systems in vehicles is to provide the best balance between ride and handling depending on the operating conditions of a vehicle. Active suspensions are far more effective over a variety of different road conditions compared to passive suspension systems. This is because of their ability to store and dissipate energy at different rates. Additionally, they can even provide energy of their own into the rest of the system. This makes active suspension systems an important topic of research in suspension systems. The biggest benefit of having an active suspension system is to be able to provide energy into the system that can minimize the response of the sprung mass. This is done using actuators. Actuator design in vehicle suspension system is an important research topic and a lot of work has been done in the field but little work has been done to estimate the peak control force and bandwidth required to minimize the response of the sprung mass. These two are very important requirements for actuator design in active suspensions. The aim of this study is estimate the peak control force and bandwidth to minimize the acceleration of the sprung mass of a vehicle while it is moving on a compliant surface. This makes the road surface a bi-lateral boundary and hence, the total system is a combination of the vehicle and the compliant road. Generalized vehicle and compliant road models are created so that parameters can be easily changed for different types of vehicles and different road conditions. The peak control force is estimated using adaptive filtering. A least mean squares (LMS) algorithm is used in the process. A case study with fixed parameters is used to show the results of the estimation process. The results show the effectiveness of an adaptive LMS algorithm for such an application. The peak control force and the bandwidth that are obtained from this process can then be used in actuator design.

Active Suspension Design Requirements for Compliant Boundary Condition Road Disturbances

Anirudh Srinivasan

GENERAL AUDIENCE ABSTRACT

Active suspension systems have been proven to be a better option compared to passive suspension systems for a wide variety of operating conditions. Active suspensions typically have an actuator system that produces a force which can reduce the disturbance caused by road inputs in the suspension. The sprung mass of a vehicle is the mass of the body and other components supported by the suspension system and the un-sprung mass is the total mass of the components which are not supported by the suspension or are part of the suspension system. The actuator is typically between the sprung mass and the un-sprung mass. When there is a single event disturbance from the road, the energy is transferred to the sprung mass, which contains the occupants, through the un-sprung mass. The actuator produces a force that reduces this acceleration in the sprung mass and hence improves ride comfort for the occupants of the vehicle. In this thesis, the single event disturbance that has been considered is a compliant road surface. This is a bi-lateral boundary since the vehicle interacts with the compliant elements under the surface of the ground. The aim of this thesis is to develop and implement a method to estimate the peak control force and bandwidth that the actuator needs to produce to eliminate or reduce the acceleration of the sprung mass which is caused by the compliant surface single event disturbance.

Acknowledgements

I would like to that my advisor, Dr. Steve Southward for giving me this opportunity to work on this research. I am thankful for his support and guidance throughout. Also, his course on Applied Linear Control gave me the foundation necessary for this research.

I would also like to thank Dr. Diana Bairaktarova and Dr. Corina Sandu for participating in my thesis committee.

I would like to thank my friends at Virginia Tech that have made this experience enjoyable and memorable.

Finally, and most importantly, I would like to thank my parents for supporting me throughout my education.

Table of Contents

List of Figures

List of Tables

1 Introduction

This chapter starts with the motivation for this research. The objectives of the study are emphasized and the approach to achieve these goals in this study have been discussed. The chapter ends with an outline of the thesis.

1.1 Motivation

Passive suspension systems are very limited since they can only store and dissipate energy at a constant rate. This makes the optimum operation range very limited. Passive suspensions cannot cope with changing road conditions and unexpected inputs to the system. Active suspension systems have come a long way in solving this problem since they can store and dissipate energy at a varying rate. They also have the ability to supply energy into the system. Sensors can be used to understand road conditions, and suspension parameters can be altered to satisfy the requirements. Active suspensions are especially very useful for discrete time operation in various conditions. This means that active suspensions can be extremely useful for vehicle operation on compliant surfaces like snow, soil or compliant bridges. Little work has been done to determine the ideal control effort in active suspensions for operation on bi-lateral compliant boundaries. This work will help in actuator designs in active suspension systems.

1.2 Objectives

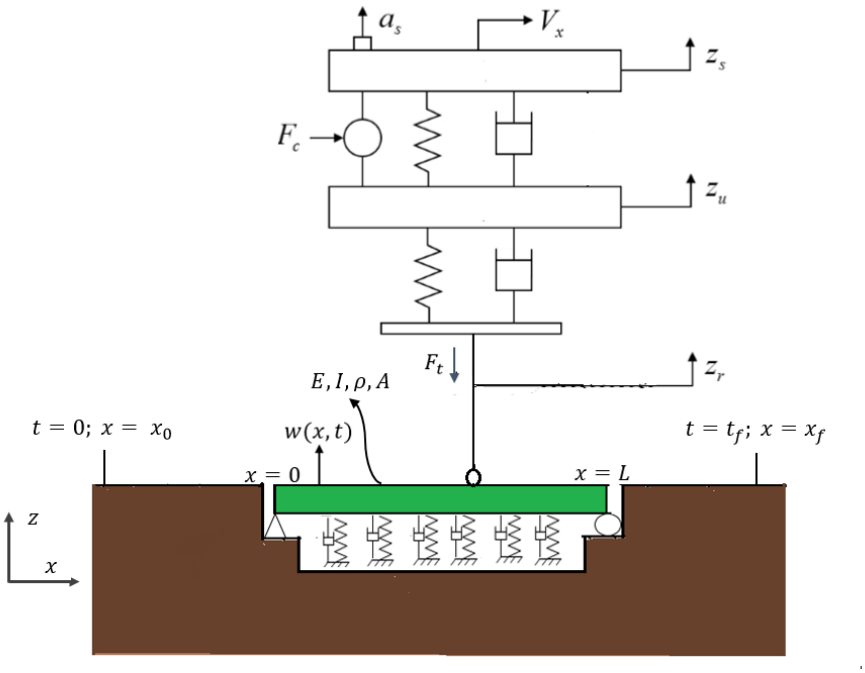

Figure 1.1: High-level model of system

In the figure 1.1, a high level representation of the model has been shown. The bi-lateral compliant road has been represented as a beam on a distributed stiffness and damping element. The quarter car with an active suspension unit has been shown moving on the model of the foundation. The vehicle travels from a non-compliant to a compliant to a non-compliant road. While the vehicle travels on the foundation, the sprung mass of the quarter car experiences acceleration. The aim of this research is to determine the peak control forces that need to be produced to eliminate the sprung mass acceleration. The approach that has been used in this research is generalized and will work for any vehicle by just tuning the suspension parameters. The results can then be used to design the right actuator system to achieve balance between ride and handling on a compliant road surface. To achieve the described objective, the approach had the following requirements:

- A vehicle model that can adequately represent all the dynamics of the system that are important for this particular problem
- A generalized model of the compliant road segment that can be easily modified for different road compliances

- Implementation of an adaptive filter to calculate the ideal control force required to eliminate sprung mass acceleration induced by the compliant road surface and estimate the bandwidth

1.3 Approach

The first step was to develop a linear quarter-car model that includes the effects of gravity. The quarter car model consists of an actuator that is assumed to be able to produce any control force and achieve any bandwidth. The next step was to develop a model for the compliant surface. It was assumed that the vehicle would have preview information of the upcoming compliant surface. The model was generalized with variable parameters. This surface would be a bi-lateral boundary condition. The next step was to combine the model of the vehicle with that of the road. The adaptive filter was implemented which could calculate the ideal control forces for optimal suspension operation.

After the development of a generalized system, parameters were chosen as a case study. A particular vehicle model was chosen with set suspension parameters. The model of the compliant surface was also determined by fixing all the model parameters. The simulation for the vehicle running on the compliant surface was run. The results were then used to extract the ideal control force which needs to be developed by the actuator for ideal operation.

1.4 Outline

This is an outline of the chapters of the thesis. The next chapter will be a literature review that talks about current active suspension systems and control techniques. The literature related to the compliant surface and adaptive filtering will also be discussed. Chapter 3 will discuss the linear quarter car model and the model of the compliant surface. These will be referred to as sub-models. Chapter 4 will discuss combination of the sub-models to obtain the plant. Chapter 5 will discuss the Fx-LMS algorithm that has been used in the study. It will talk about the details involved and tuning of the parameters. Chapter 6 will discuss the results of the study. Chapter 7 will contain the conclusions and scope for future work.

2 Literature Review

This chapter discusses the existing active suspension systems and the control techniques involved. This will be the background for the model used in this research. This literature review will also discuss the background for the compliant road model. A modification of this model has been used in this research.

2.1 Active Vehicle Suspension Systems

Active suspensions can dissipate energy at a variable rate. Also, suspension parameters can be changed to improve operation depending on conditions. This makes active suspensions considerably superior to passive suspensions. This has been established by Sharp and Crolla [1] in their review of system design for road vehicle suspensions. The design of suspension systems is essentially a trade-off between handing and ride of the vehicle. This has been emphasized in the research by Tseng and Hrovat [2]. Actuator design is one of the major challenges in the design of active suspension systems. An estimate of the peak control force and the bandwidth are the main requirements for the design of an actuator. Little work has been done to estimate the peak control force and bandwidth required by an active suspension system for optimum operation. A recent work by Rao [3] aims at estimating peak control force and bandwidth when the vehicle encounters a single event disturbance on the road. But the work is limited to a road surface which is a unilateral boundary. There has been a lot of research on electromagnetic [4,5] and hydraulic actuators [6] for active suspension design. The work is focused on the evaluation of performance of actuators and not selection of actuators using the peak control force and bandwidth.

Research has been done on various types of control techniques. Some of these control techniques are Fuzzy control, Optimal Control, neural control and preview control as reviewed in [7]. Thompson [8] demonstrated the use of optimal control which places constraints on vehicle response to road excitations. Ting, Li [9] designed the fuzzy controller for active suspension systems. Nguyen, Bui [10] designed hybrid controllers which used H∞ for robustness and adaptive controls for non-linearity of the actuators. All this research focused on improving control systems to improve the trade-off between ride and handling in vehicles. However, this work was not focused on the estimation of ideal control forces that the actuators must produce for ideal operation

of the vehicle. Rao [3] has done research on this but it only focuses on single-event disturbances where the surface is non-compliant.

Preview information is an important factor that is considered in this thesis. Preview information in active suspensions was introduced by Bender [11]. He showed that preview can improve the performance of active suspension systems significantly. Tomizuka [12] showed in his research that the form of preview control depends on the roadway spectrum and vehicle speed. Preview information can be obtained in different ways. It can be obtained using information from sensors at the front of the vehicle. Input to the front of the vehicle can be used as preview for the input into the rear wheels of the vehicle [13]. In a military convoy, preview information can be obtained from the vehicle in the front [14]. Preview allows the control system to start functioning before the event occurs. Also, other than improving ride, preview can also reduce power requirements since the peak control force required at the event might be lower [15]. In this research, preview control is not used in real-time. Instead it is used offline and iteratively.

2.2 Winkler Foundation

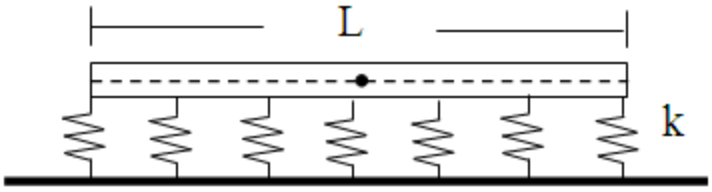

Figure 2.1: Winkler Foundation

The Winkler Foundation [16] is a model of a beam on an elastic foundation. It was named after Emil Winkler who was the first to solve a problem of a beam on an elastic foundation. The Winkler foundation has been discussed as a possible solution for modeling of soil and other compliant surfaces [17]. The Winkler foundation with a minor modification has been used to model the compliant surface in this study. The model for the compliant surface in this study uses a Winkler foundation with damping elements in parallel with the stiffness elements shown in figure 2.1. This will be further discussed in later Sections.

2.3 Adaptive Filtering

Methods of adaptive filtering have already been developed [18]. Rao [3] has discussed the application of adaptive filters to vehicle suspension in detail but for a different objective. Adaptive filters have also been used for system identification [19].

In this study, the aim is to reduce the response of the suspension system's sprung mass while the vehicle travels on a compliant surface, by producing a control force. This estimation of the control force is done using adaptive filtering. The aim of this work is not to develop new control laws but to implement adaptive filtering to estimate the ideal control force that needs to be produced by the actuator of an active suspension system. This has been done offline and using an iterative process.

3 Description of Sub-Models

The complete model consists of two components. One of them is the model for the vehicle which includes the active suspension system, while the other component is the model of the road surface. For active suspension design to improve ride, vertical dynamics in the suspension is of most interest. This makes the quarter car model very attractive for use in this study. The quarter car model can be used to develop the system and the results can be used for implementation on a vehicle model with a higher degree of freedom.

3.1 Quarter-car Model

As discussed above, the quarter car model has been used to simulate the vehicle response for inputs into the suspension system.

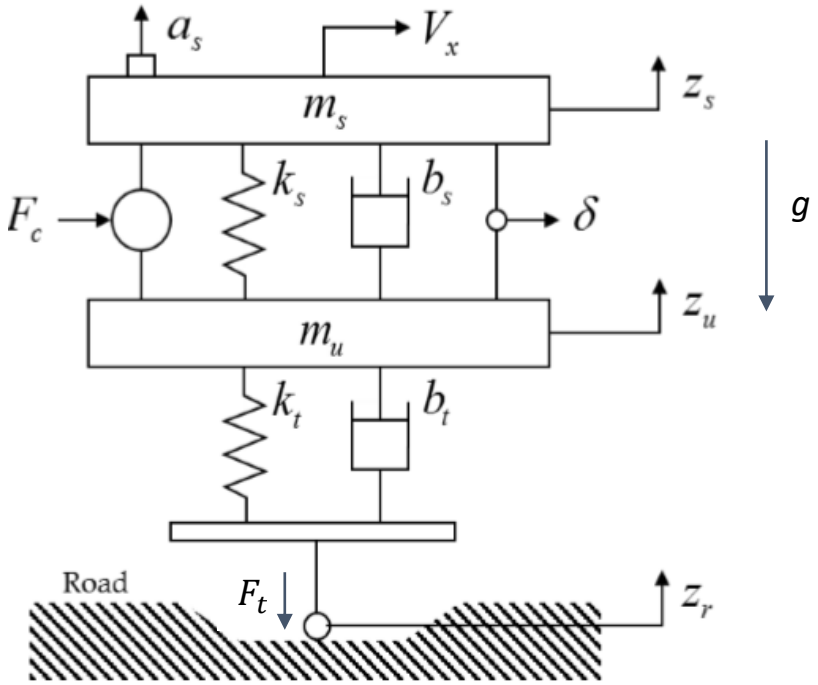

Figure 3.1: Quarter Car model

Figure 3.1 shows a schematic diagram of the quarter car model that was used in this study.

m_s and m_u are the sprung and un-sprung masses respectively. k_s and k_t are the spring constants of the suspension and the tire respectively. b_s and b_u are the damping coefficients of the suspension and tire respectively. V_x is the linear velocity of the quarter car. z_r is the vertical displacement as

a result of the road profile and z_u and z_s are the vertical displacements of the un-sprung and sprung masses respectively. a_s is the acceleration of the sprung mass. δ is the displacement between the sprung and the un-sprung masses. F_t is the tire force generated by the quarter car at the tire. g is the acceleration due to gravity. F_c is the control force that is applied to the suspension system and the force is applied between the sprung and un-sprung masses.

It has been assumed that the actuator which produces the control force is ideal. Thus, it can produce any control force and has unlimited bandwidth. This model is completely linear. The tire is always in contact with the road surface and there is no lift-off. There is point contact between the tire and the road. Also, it is assumed that all the parameters of the quarter car are known.

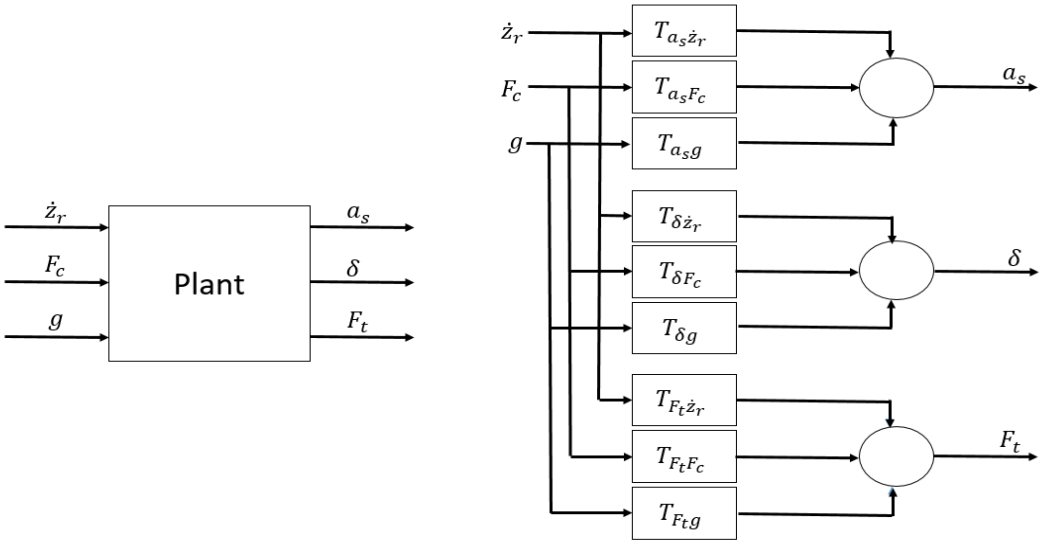

Figure 3.2: Inputs and Outputs of Quarter Car

From figure 3.2, we can see that the inputs to the quarter car are $(\dot{z}_r, F_c, g)$ and the outputs are (a_s, g, F_t). It should be noted that gravity is treated as an input to the system in the model. Also, $\dot{z}_r$, the vertical velocity is used as an input to the quarter car instead of the vertical displacement. This is because the tire is modeled with a damper and hence it requires a velocity input. Also, from figure 3.2, $T_{a_s\dot{z}_r}$, $T_{a_sF_c}$, T_{a_sg}, $T_{\delta\dot{z}_r}$, $T_{\delta F_c}$, $T_{\delta g}$, $T_{F_t\dot{z}_r}$, $T_{F_tF_c}$ and T_{F_tg} are the respective transfer functions of the various input-output paths.

$$x_1 = z_s$$

$$x_2 = \dot{z}_s$$

$$x_3 = z_u \tag{3.1}$$

$$x_4 = \dot{z}_u$$

$$x_5 = z_r$$

The equations in 3.1 are the states that have been used for the state space representation. The vertical displacement as a result of the road is a state while the corresponding velocity is an input into the system.

$$\dot{x}_1 = x_2$$

$$\dot{x}_2 = -\frac{k_s}{m_s}x_1 - \frac{b_s}{m_s}x_2 + \frac{k_s}{m_s}x_3 + \frac{b_s}{m_s}x_4 + \frac{F_c}{m_s} - g$$

$$\dot{x}_3 = x_4 \tag{3.2}$$

$$\dot{x}_4 = \frac{k_s}{m_u}x_1 + \frac{b_s}{m_u}x_2 + \frac{-k_s - k_t}{m_u}x_3 + \frac{-b_s - b_t}{m_u}x_4 + \frac{k_t}{m_u}x_5 + \frac{b_t}{m_u}\dot{z}_r - \frac{F_c}{m_u} - g$$

$$\dot{x}_5 = \dot{z}_r$$

The equations in 3.2 are the state space equations of the quarter car model for the inputs and outputs described above. To simulate this in MATLAB, this must be in the following form,

$$\{\dot{x}\} = [A]\{x\} + [B]\{u\}$$

$$\{y\} = [C]\{x\} + [D]\{u\} \tag{3.3}$$

The state space equations in 3.2 are represented in the matrix form below.

$$\begin{Bmatrix} \dot{x}_1 \\ \dot{x}_2 \\ \dot{x}_3 \\ \dot{x}_4 \\ \dot{x}_5 \end{Bmatrix} = \begin{bmatrix} 0 & 1 & 0 & 0 & 0 \\ -\frac{k_s}{m_s} & -\frac{b_s}{m_s} & \frac{k_s}{m_s} & \frac{b_s}{m_s} & 0 \\ 0 & 0 & 0 & 1 & 0 \\ \frac{k_s}{m_u} & \frac{b_s}{m_u} & \frac{-k_s-k_t}{m_u} & \frac{-b_s-b_t}{m_u} & \frac{k_t}{m_u} \\ 0 & 0 & 0 & 0 & 0 \end{bmatrix} \begin{Bmatrix} x_1 \\ x_2 \\ x_3 \\ x_4 \\ x_5 \end{Bmatrix} + \begin{bmatrix} 0 & 0 & 0 \\ 0 & \frac{1}{m_s} & -1 \\ 0 & 0 & 0 \\ \frac{b_t}{m_u} & -\frac{1}{m_u} & -1 \\ 1 & 0 & 0 \end{bmatrix} \begin{Bmatrix} \dot{z}_r \\ F_c \\ g \end{Bmatrix}$$

$$\begin{Bmatrix} y_1 \\ y_2 \\ y_3 \end{Bmatrix} = \begin{bmatrix} -\frac{k_s}{m_s} & -\frac{b_s}{m_s} & \frac{k_s}{m_s} & \frac{b_s}{m_s} & 0 \\ 1 & 0 & -1 & 0 & 0 \\ 0 & 0 & k_t & b_t & -k_t \end{bmatrix} \begin{Bmatrix} x_1 \\ x_2 \\ x_3 \\ x_4 \\ x_5 \end{Bmatrix} + \begin{bmatrix} 0 & \frac{1}{m_s} & -1 \\ 0 & 0 & 0 \\ -b_t & 0 & 0 \end{bmatrix} \begin{Bmatrix} \dot{z}_r \\ F_c \\ g \end{Bmatrix} \quad (3.4)$$

The equations in 3.4 are the state space equations in matrix form and they can be simulated in MATLAB.

Table 3.1: Values of Parameters in Quarter car model

Parameter	Value	Unit
m_s	400	kg
m_u	40	kg
k_s	21000	N/m
k_t	150000	N/m
b_s	1500	Ns/m
b_t	250	N/m

The values of the parameters chosen for the quarter car are shown in the table 3.1. The values have been chosen to represent a typical passenger car.

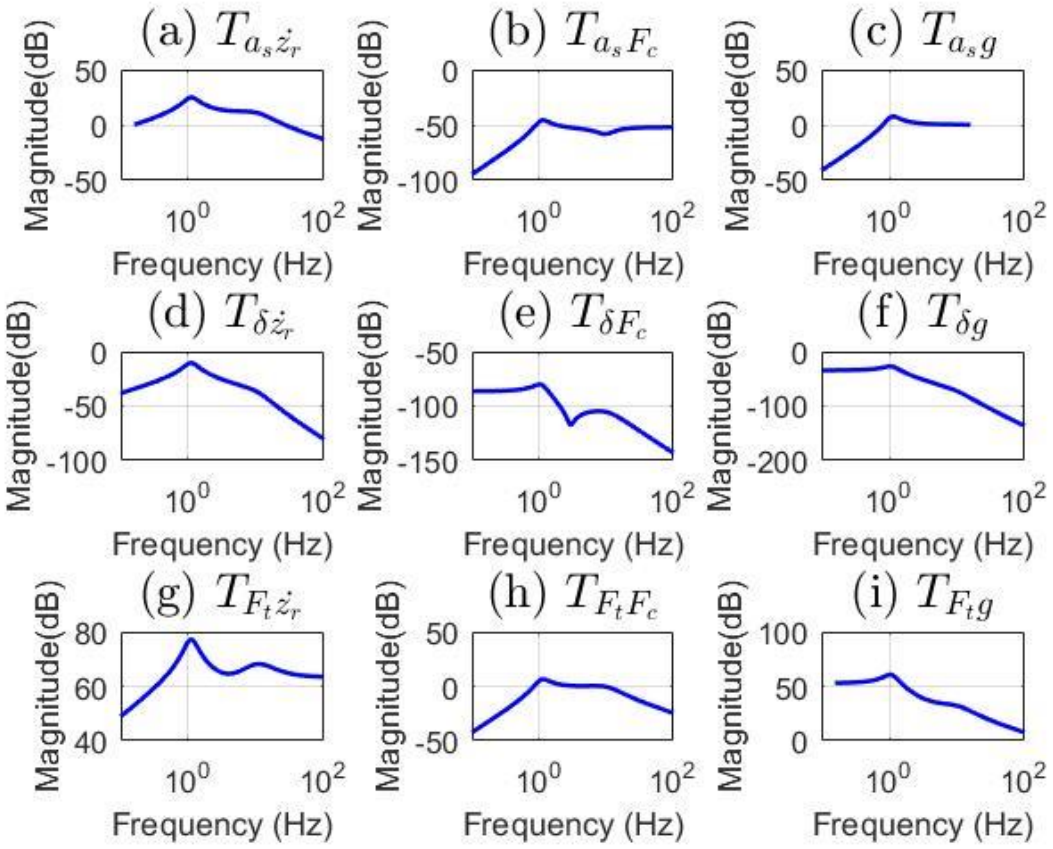

Figure 3.3: Transfer Functions of Quarter car model

Figure 3.3 shows the frequency response of each path with the chosen parameters from table 3.1. The code was developed on MATLAB and the parameters can be easily changed to get the model for any vehicle.

3.2 Compliant Road Surface Model

The compliant surface model used in this study is a minor modification of the Winkler foundation which is discussed in [16]. The Winkler foundation is the model of a beam on an elastic foundation and it is used for modeling soil and other compliant surfaces. The model used in this research consists of damping elements along with the stiffness elements. This model will be referred to as the Modified Winkler Foundation in this study.

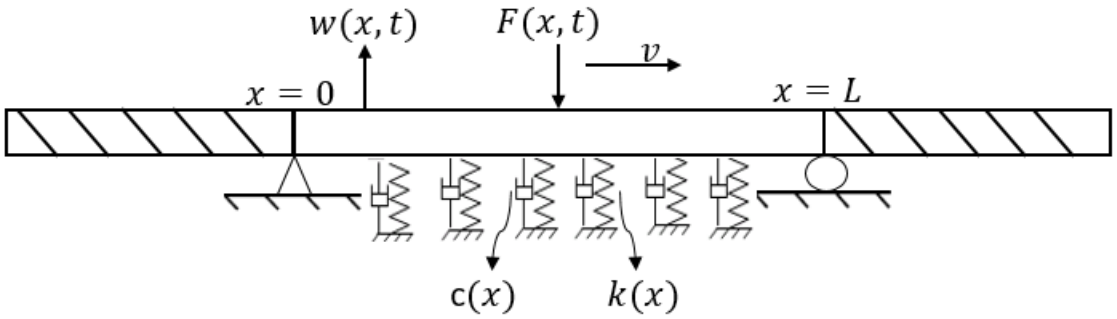

Figure 3.4: Model of the Modified Winkler Foundation

The figure 3.4 represents the model that has been used for the compliant road surface in this study. The compliant surface is represented as a simply supported beam with a damped, elastic foundation starting at $x = 0$ and ending at $x = L$. $w(x,t)$ is the displacement of the beam due to applied force, $F(x,t)$. v is the velocity of the vehicle moving on the beam. $c(x)$ is the coefficient of damping on the damping elements as a function of position on the beam. $k(x)$ is the spring constant of the stiffness elements as a function of position of beam. This allows to have variable stiffness and damping in the foundation.

Based on the figure 3.4, the model of the Modified Winkler Foundation would be the following.

$$EI\frac{\partial^4 w(x,t)}{\partial x^4} + \rho A\frac{\partial^2 w(x,t)}{\partial t^2} + k(x)w(x,t) + c(x)\frac{\partial w(x,t)}{\partial t} = F(t)\delta\big(x - v(t - t_0)\big) \quad (3.5)$$

In equation 3.5, E is the Young's modulus of the beam. I is the second moment of inertia of the beam. ρ is the density of the beam. A is the area of the beam. t is the time at the current position of the vehicle and t_0 is the time at $x = 0$.

The boundary conditions of the beam are the following.

$$w(0,t) = w(l,t) = 0$$

$$\frac{\partial^2 w(0,t)}{\partial x^2} = \frac{\partial^2 w(l,t)}{\partial x^2} = 0 \quad (3.6)$$

The initial conditions of the beam are defined below.

$$w(x,0) = w_0(x) = 0; w_t(x,0) = \dot{w}_0(x) = 0 \quad (3.7)$$

After defining the equation of the model and the boundary and initial conditions, the next step would be to solve the equations of the beam. Let us assume the following solution.

$$w(x,t) = \sum_{n=1}^{N} T_n(t) Sin\left(\frac{n\pi x}{L}\right) \tag{3.8}$$

The solution has a spatial component and a temporal component. Here, N is the number of nodes and $n = 1,2,3,..,N$.

Substituting this assumed solution into equation 3.5, we get the following.

$$\sum_{n=1}^{N}\left[\left\{EI\left(\frac{n\pi}{L}\right)^4 + k\right\}T_n(t) + \rho A\ddot{T}_n(t) + c\dot{T}_n(t)\right] Sin\left(\frac{n\pi x}{L}\right) = F(t)\delta\big(x - v(t - t_0)\big) \tag{3.9}$$

Now, multiplying both sides with the wave function for mode 'm',

$$\sum_{n=1}^{N}\int_0^L \left[\left\{EI\left(\frac{n\pi}{L}\right)^4 + k\right\}T_n(t) + \rho A\ddot{T}_n(t) + c\dot{T}_n(t)\right] Sin\left(\frac{n\pi x}{L}\right) Sin\left(\frac{m\pi x}{L}\right)$$

$$= F(t)\int_0^L \delta\big(x - v(t - t_0)\big) Sin\left(\frac{m\pi x}{L}\right) dx \tag{3.10}$$

Due to orthogonality of the modes,

$$\sum_{n=1}^{N}\int_0^L Sin\left(\frac{n\pi x}{L}\right) Sin\left(\frac{m\pi x}{L}\right) dx = \frac{L}{2}\ if\ n = m$$

$$\sum_{n=1}^{N}\int_0^L Sin\left(\frac{n\pi x}{L}\right) Sin\left(\frac{m\pi x}{L}\right) dx = 0\ if\ n \neq m \tag{3.11}$$

Thus equation 3.10 can be reduced to the following solution.

$$\left[\frac{L}{2}EI\ \left(\frac{m\pi}{L}\right)^4 + K_m\right] T_m(t) + \frac{\rho AL}{2}\ddot{T}_m(t) + C_m\dot{T}_m(t) = F(t)\ Sin\left(\frac{m\pi v(t - t_0)}{L}\right) \tag{3.12}$$

In equation 3.12,

$$K_m = \sum_{n=1}^{N} \int_0^L k(x) Sin\left(\frac{n\pi x}{L}\right) Sin\left(\frac{m\pi x}{L}\right) dx$$

$$C_m = \sum_{n=1}^{N} \int_0^L c(x) Sin\left(\frac{n\pi x}{L}\right) Sin\left(\frac{m\pi x}{L}\right) dx \tag{3.13}$$

The initial conditions are,

$$T_m(0) = \dot{T}_m(0) = z; for\ m = 1,2,3, \dots, N \tag{3.14}$$

The solution described in equation 3.12 is for a moving vehicle, that is when $v > 0$. The solution for a stationary vehicle, $v = 0$, has been described below.

$$\left[\frac{L}{2} EI \left(\frac{m\pi}{L}\right)^4 + K_m\right] T_m(t) + \frac{\rho AL}{2} \ddot{T}_m(t) + C_m \dot{T}_m(t) = F(t)\, Sin\left(\frac{m\pi x_p}{L}\right) \tag{3.15}$$

Here, x_p is the position of the stationary vehicle on the beam. The definitions of C_m and K_m are as defined in equation 3.13. Also, the initial conditions are the same as in 3.14.

Table 3.2: Values of Parameters in Compliant surface model

Parameter	**Value**	**Unit**
L	3	m
A	0.002	m^2
ρ	7850	kg/m^3
E	200×10^9	Pa
k	15000	N/m
c	0.5	Ns/m

The input to the beam is the tire force, F_T of the vehicle. The output of the beam is the velocity of the beam, $\dot{z}_r$ which is basically the velocity of the road that acts as an input to the quarter car. The transfer function of the compliant surface is shown below.

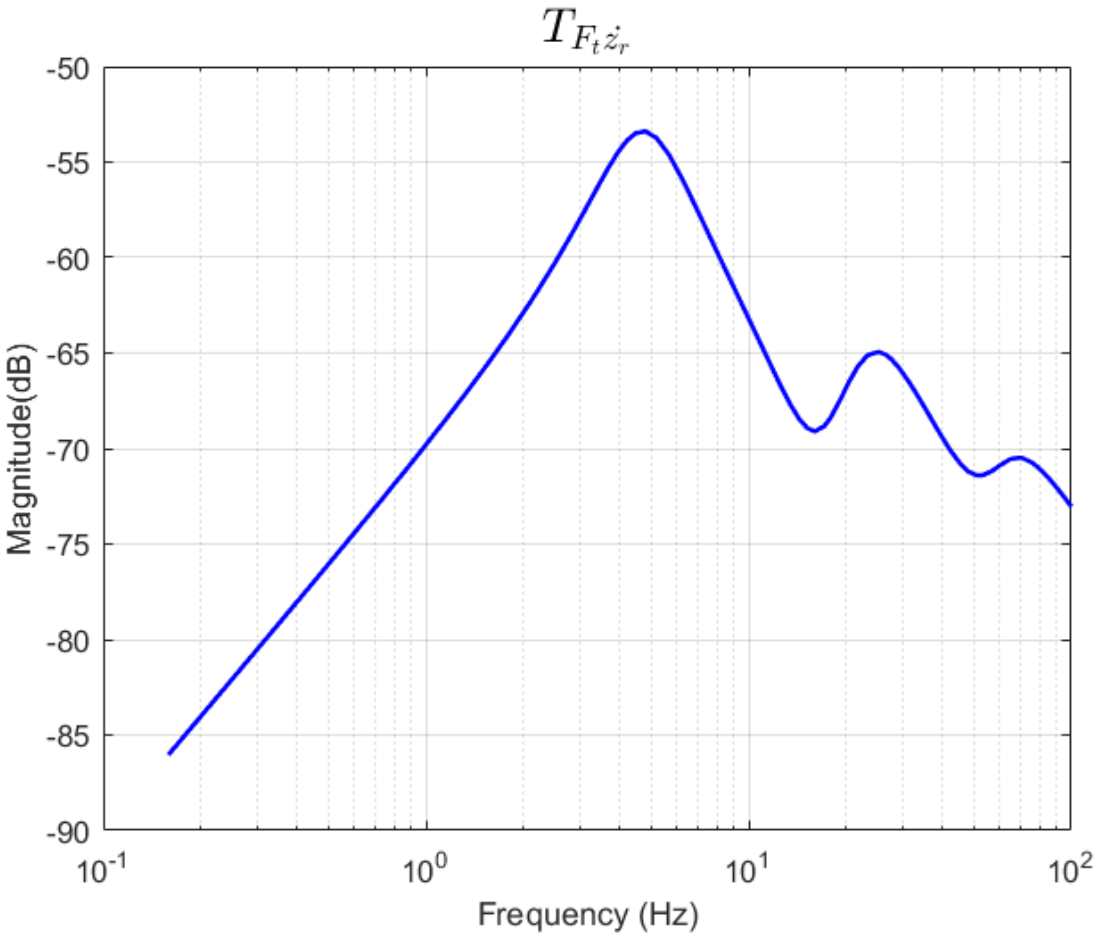

Figure 3.5: Transfer function of Compliant surface

Figure 3.4 shows the frequency response of the model of the foundation using chosen parameters from table 3.2. The code was developed on MATLAB and the parameters can be easily changed for different possible models of the compliant surface. In this research, it is assumed that all the parameters for this model of the foundation are known.

4 Combination of Sub-Models

Section 3 describes the two sub-models, which are the quarter car model and the model of the compliant surface. The objective is to estimate the peak control force required for optimal operation of a vehicle on a compliant surface. Thus, to complete the model for this study, the two sub-models need to be combined to obtain the plant model.

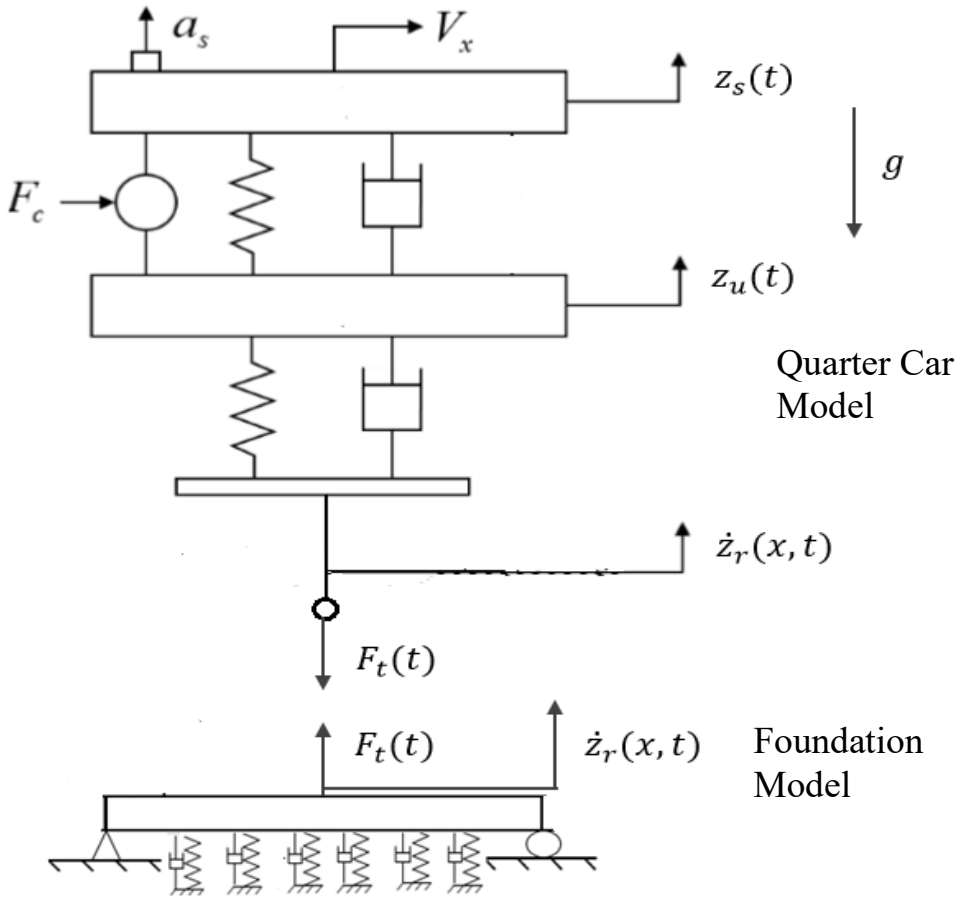

Figure 4.1: Modeling Challenge

Figure 4.1 shows the modeling challenge in this research. As discussed earlier, the vehicle is moving on the model of the foundation and this causes a sprung mass acceleration. The quarter car is represented by an ordinary differential equation and the foundation is represented by a partial differential equation, and these two models have to be combined to get the complete model of the system. As we can see in the figure 4.1, $F_t(t)$ is the tire force, which is an output of

the quarter car and $\dot{z}_r(x,t)$ is the velocity input to the quarter car from the foundation. Thus, the quarter car gives an input to the foundation and the foundation then gives an input to the quarter car, which closes the system.

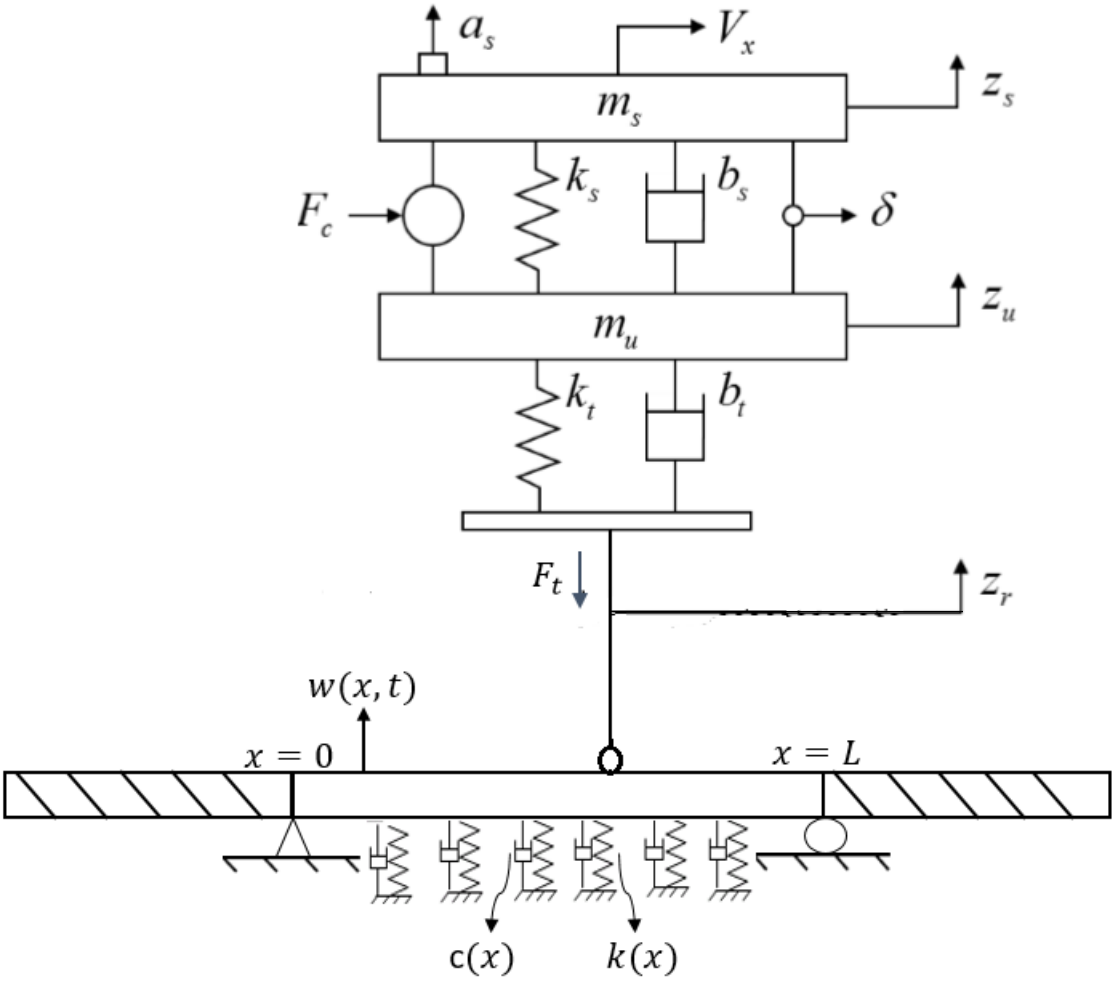

Figure 4.2: Plant model

The model of the plant has been shown in figure 4.2. This is a combined model of the quarter car and the compliant surface. All the elements of the model and the terminologies used have been described in the previous section.

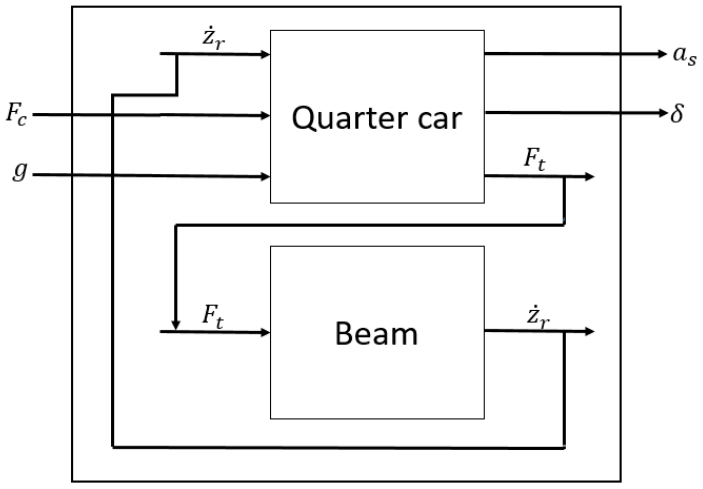

Figure 4.3: Inputs and Outputs of the plant

The inputs of this model are (F_c, g). F_c is the control force that is applied between the sprung and un-sprung masses. g is the acceleration due to gravity which is considered to be an input to the system. The outputs are (a_s, δ). a_s is the acceleration of the sprung mass and δ is the relative displacement between the sprung and un-sprung masses. From figure 4.3, we can see that F_t and $\dot{z}_r$ are internal inputs and outputs of the sub-models but are not present as inputs and outputs of the complete plant. Though the plant shown in figure 4.3 has multiple inputs and outputs, we only consider one path in this study which is from F_c to a_s.

This model was made in two stages. The first stage was to create and simulate a model for a stationary vehicle.

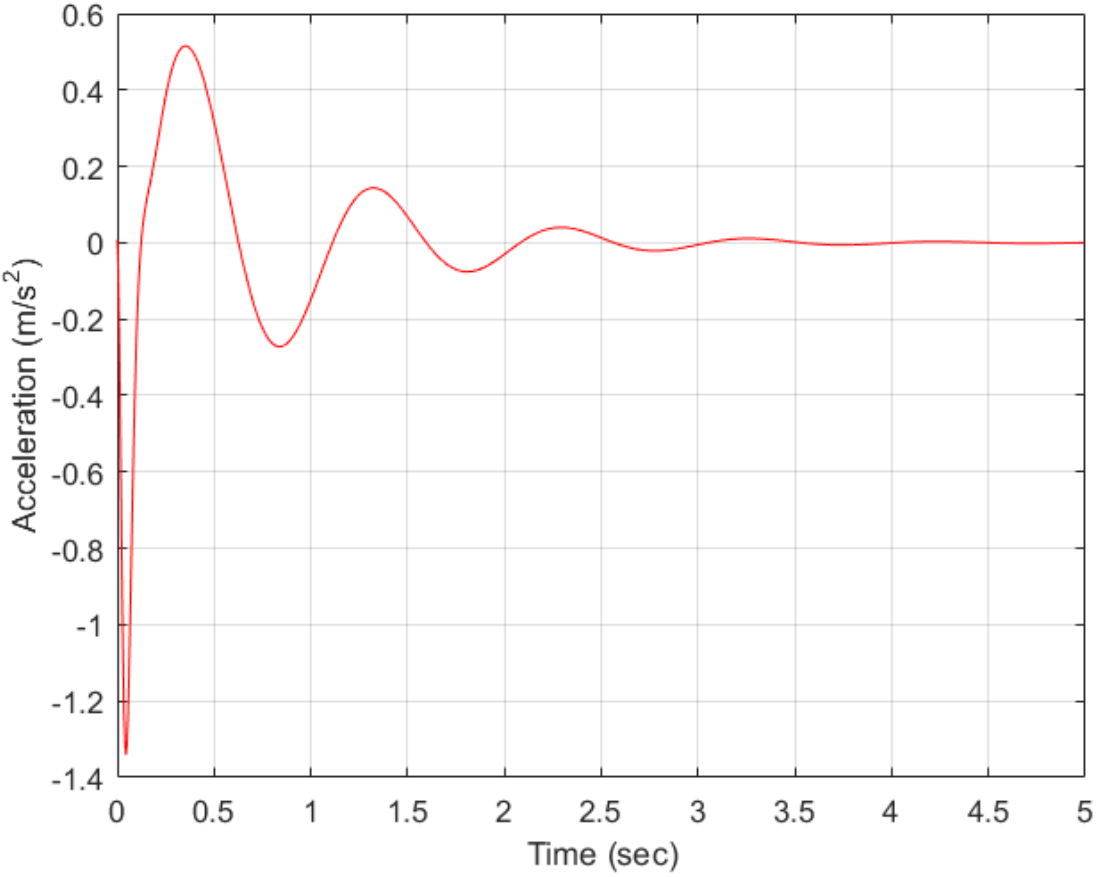

Figure 4.4: Simulation for quarter car in the middle of the beam without control

The plot in figure 4.4 shows the uncontrolled response of a quarter car that is placed in the middle of the beam. The car has a velocity of zero and the acceleration is due to the springs being pre-loaded due to gravity. In figure 4.4, we can see that that the sprung mass achieves a peak acceleration of about $-1.35\ m/s^2$ and then slowly settles at zero.

The next stage in the study was to allow the quarter car to have a forward velocity ($v > 0$) and the response was simulated.

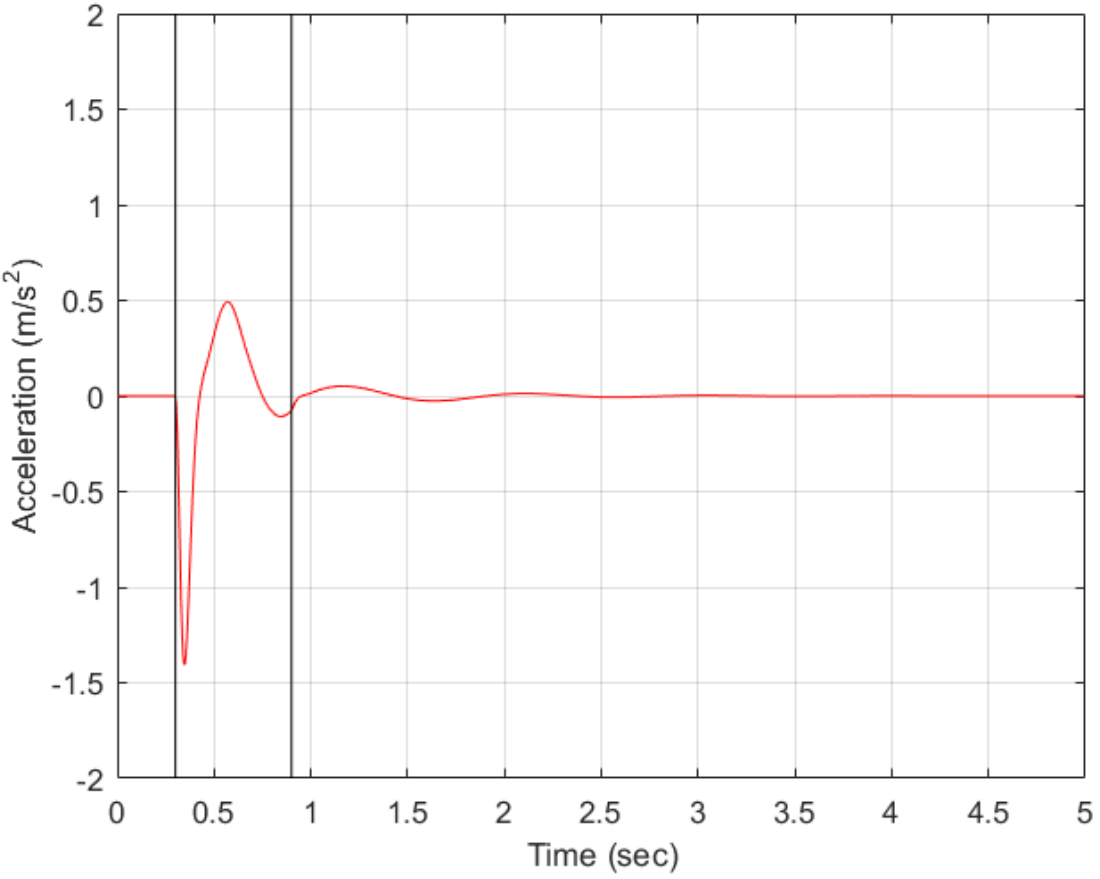

Figure 4.5: Simulation for a moving quarter car without control

The simulation of the plant in figure 4.5 is for a quarter car which has a non-zero velocity. This simulation was with gravity turned on and with no control. The vertical black lines represent the beginning and the end of the compliant surface. There is a pre-view period of 0.3 seconds before the quarter car reaches the compliant surface. The quarter moves on this foundation for the next 0.6 seconds before returning to non-compliant road conditions. The peak acceleration is achieved as soon as the quarter car reaches the compliant surface. The peak acceleration is achieved at 0.35 seconds and then the sprung mass slowly starts to attain equilibrium. For the simulations in figure 4.4 and 4.5, stiffness and damping have been chosen as a function of position as an attempt to replicate different conditions on the road. All parameters used other than stiffness and damping are the same as in tables 3.1 and 3.2. The stiffness constant and damping ratio values have been shown below.

$$k = \begin{cases} 15000\ N/m\,;\ 0.3 \le x \le 0.45 \\ 3000\ N/m\,; 0.45 < x \le 0.75 \\ 15000\ N/m\,; 0.75 < x \le 0.9 \end{cases}$$

$$c = \begin{cases} 0.9\ Ns/m\,;\ 0.3 \le x \le 0.45 \\ 0.3\ Ns/m\,; 0.45 < x \le 0.75 \\ 0.9\ Ns/m\,; 0.75 < x \le 0.9 \end{cases} \qquad (4.1)$$

5 Ideal Control Force Estimation

The objective of this study is to estimate the peak control force required for optimal operation of a vehicle on a compliant surface. Thus, the response of the system due to the disturbance is to be minimized and this needs to be done offline. Adaptive filters are perfect for this application.

Adaptive filters use a cost function to minimize the response. The optimization depends on the choice of the cost function. The plant in this study has acceleration and displacement as outputs. This study only focuses on sprung mass acceleration response and hence that has been chosen for use in the cost function. The following cost function is used,

$$J(F_c) = \left(\frac{1}{T}\right) \int_{event} a_s^2(t)dt \qquad (5.1)$$

The choice of acceleration in the cost function helps estimate a control force that will minimize the response. This will improve the ride performance of the quarter car since the vertical acceleration response will be curbed. Other cost functions can be chosen to control different types of responses or to improve certain aspects of vehicle performance. The cost function in equation 5.1 has been chosen for this specific application.

In this study, the method used for the estimation of the peak control force is Filtered-X-LMS algorithm, which is an extension of LMS optimization method.

5.1 LMS Optimization

The aim of LMS optimization is to minimize the error between the output signal and the desired signal. This has been explained in detail in [18]. This is done using an ideal filter.

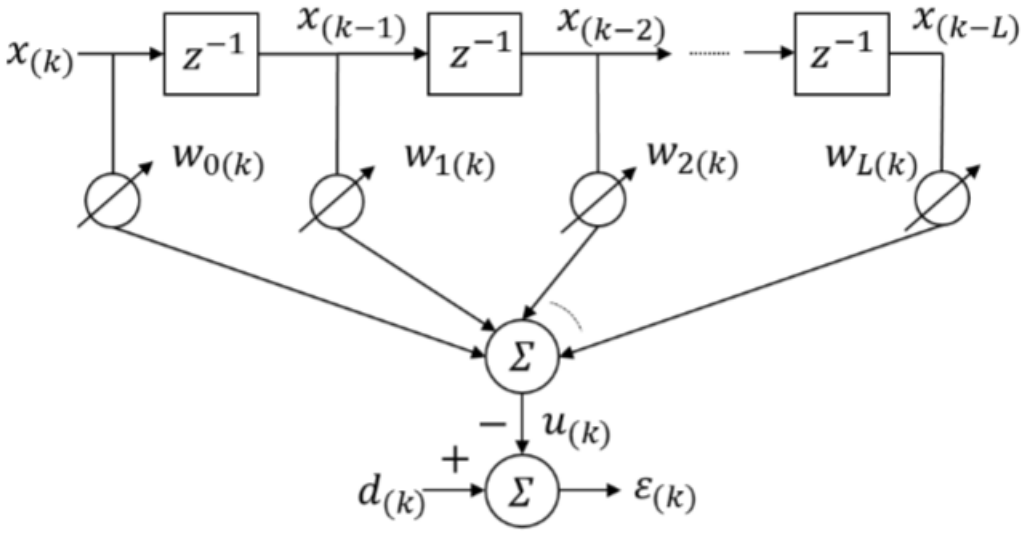

Figure 5.1: Adaptive Linear combiner

Figure 5.1 shows an adaptive linear combiner and it explains the basic process involved in adaptive filtering. This is a non-recursive digital filter. $x_{(k)}$ is the input signal vector and it has the elements $x_{(k-1)}, x_{(k-2)}, \dots, x_{(k-L)}$. L is the length of the filter which contains the elements $w_{o(k)}, w_{1(k)}, w_{2(k)}, \dots, w_{L(k)}$. The weights are adjustable and have their corresponding elements in the control signal. The summing junction in figure 5.1 sums the products of the weights and their corresponding element in the input signal to produce $u_{(k)}$, which is the output signal. Here, (k) represents the k^{th} time index in discrete time. The output signal, $u_{(k)}$ is subtracted from the desired signal, $d_{(k)}$ to produce the error signal, $\varepsilon_{(k)}$. This error signal is to be reduced in an adaptive process.

$$\varepsilon_{(k)} = d_{(k)} - u_{(k)} \tag{5.2}$$

Equation 5.2 is a representation of the process to obtain the error signal. Here,

$$u_{(k)} = \sum_{l=0}^{L} w_{l(k)} x_{(k-l)} \tag{5.3}$$

Equation 5.3 shows the summing process in the linear combiner. For a fixed set of weights, the output is a linear combination of the inputs.

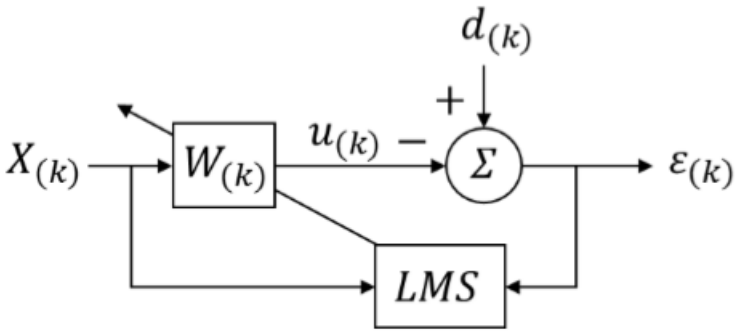

Figure 5.2: LMS algorithm

Figure 5.2 represents the LMS adaptive algorithm which is obtained from the linear combiner in figure 5.1. The LMS algorithm is used to reduce the error signal that is obtained from equation 5.2. The adjustable weights are adapted using this LMS algorithm. The weights for the next time index, $w_{(k+1)}$ are obtained using a gradient descent method.

$$W_{(k+1)} = W_{(k)} + \mu\varepsilon_{(k)}X_{(k)} \tag{5.3}$$

The equation for the process used to calculate the weights is equation 5.3. μ is a gain constant and it controls the spend and stability of the adaptation process. The choice of the gain constant is by trial and error and must be optimized for efficient operation of the algorithm.

Filtered-X-LMS algorithm has been used in this study which is an extension of the LMS algorithm.

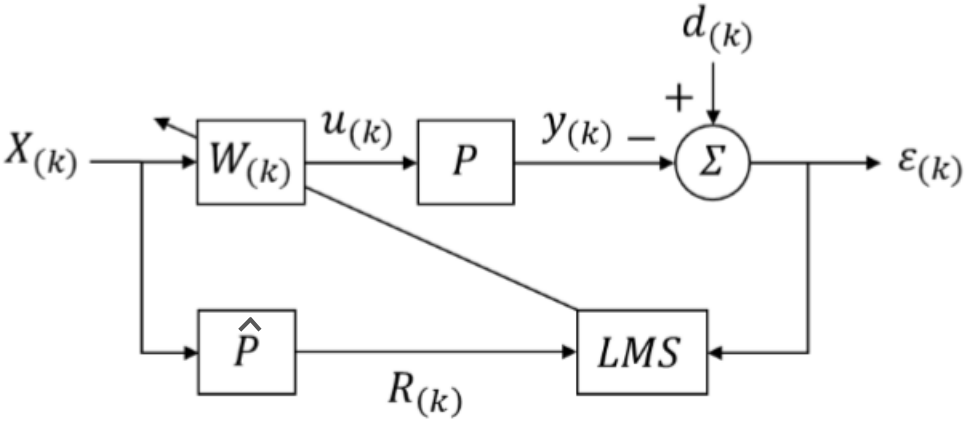

Figure 5.3: Filtered-X-LMS algorithm

We can see in figure 5.3 that a dynamic system, or the plant exists after the block which represents the adaptive filter. This is a different case from the representation in figure 5.2 and this requires a Fx-LMS algorithm.

In this process, the input signal, $X_{(k)}$ is filtered by the plant model, P and is then used in the LMS algorithm. The next set of weights, $w_{(k+1)}$ is calculated using the gradient descent method.

$$W_{(k+1)} = W_{(k)} + \mu\varepsilon_{(k)}R_{(k)} \tag{5.4}$$

$R_{(k)}$ the new input vector that is obtained by exciting the plant dynamics using an input excitation signal. The choice of the input excitation signal is an important factor to excite the plant dynamics completely and in the adaptation process. The Fx-LMS converges to de-correlate the error signal from the desired signal.

5.1.1 Iterations in Fx-LMS adaptation

The Fx-LMS adaptation process has been discussed in 5.1. The gradient descent method is used to estimate the next set of weights of the filter so that the error signal can be minimized. When a batch of inputs is used as the input signals, a batch of weights can be estimated for the filter. The filter may have any initial conditions. For the next iteration, the current weights can be used as the initial conditions to calculate the next set of weights for the filter. This is an iterative process and Fx-LMS performs better with higher number of iterations. But if the number of iterations are too high, the time taken might be too much for a real-time control system. Since the estimation in this study is offline, the choice of the number of iterations is not a constraint.

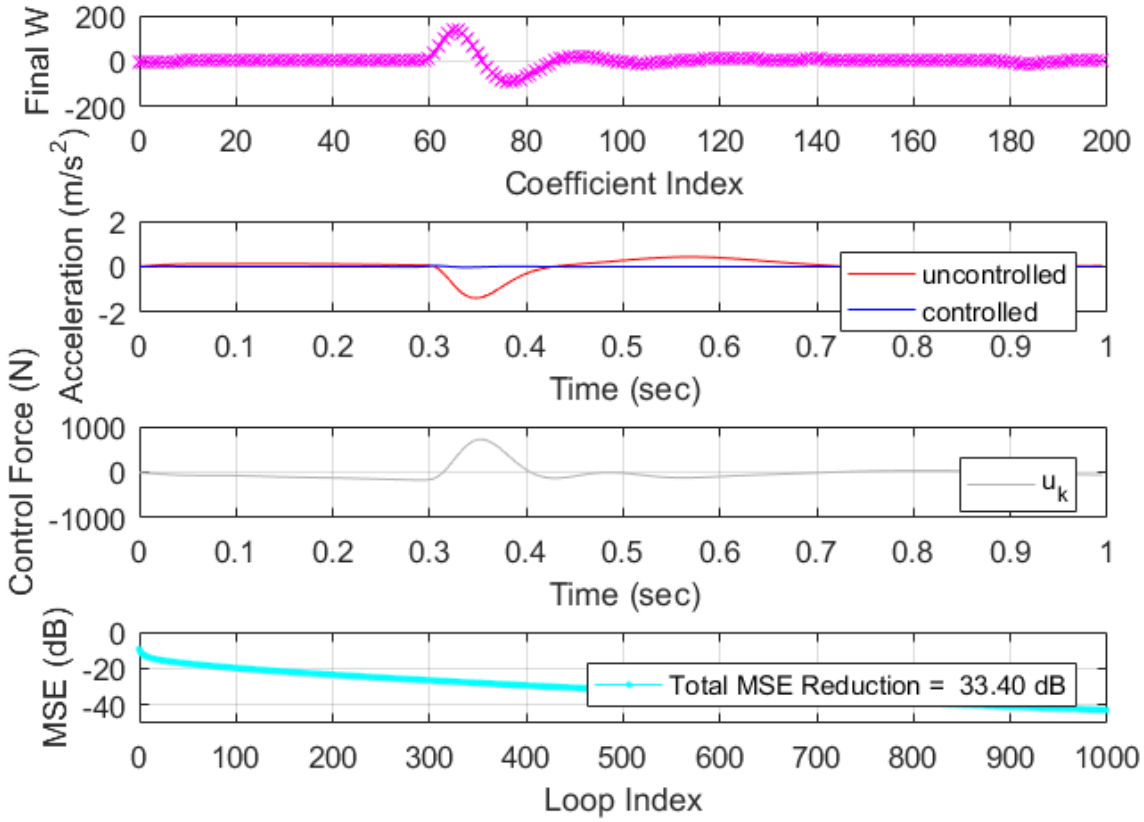

Figure 5.4: Sample iterative Fx-LMS adaptation with 1000 iterations

The figure 5.4 shows a sample result of an iterative Fx-LMS adaptation process with 1000 iterations. The plant was simulated with control. The length of the filter was fixed. The gain constant was fixed and the adaptation was run on MATLAB. We can see that the total reduction in mean square error is about 20 dB at the end of 100 iterations and the reduction at the end of 1000 iterations is 33.40 dB. We can see that a higher number of iterations increases the total mean square error reduction. Though the amount of time to complete the adaptation process also increases, this is not a constraint since the LMS adaptation in this study is offline.

5.1.2 Choice of gain constant in Fx-LMS adaptation

The gain constant or the step size controls the rate at which the adaptive filter converges. This can be seen in equation 5.4. To see the effect of the choice of gain constant, the adaptation process was run for the plant with control and the total mean square error reductions were compared for the

two different gain constants. All parameters other than the gain constant were the same for both simulations.

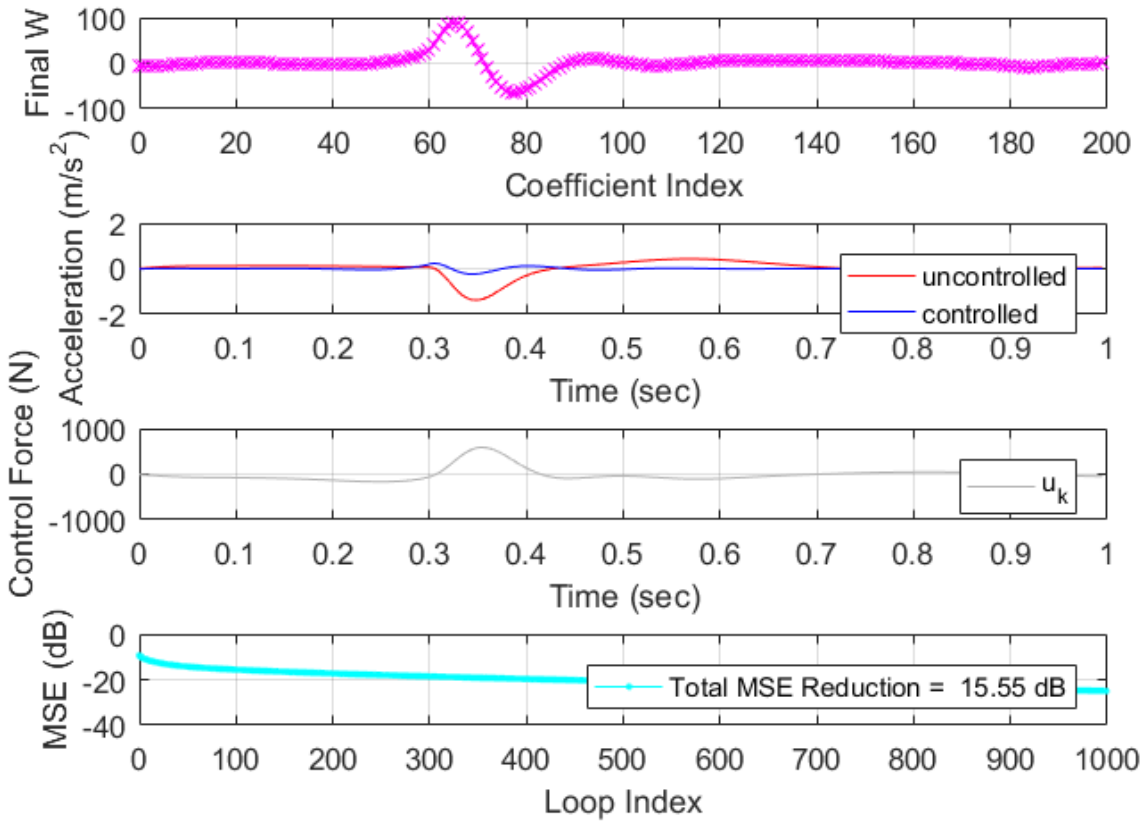

Figure 5.5: Sample iterative Fx-LMS adaptation with lower gain constant

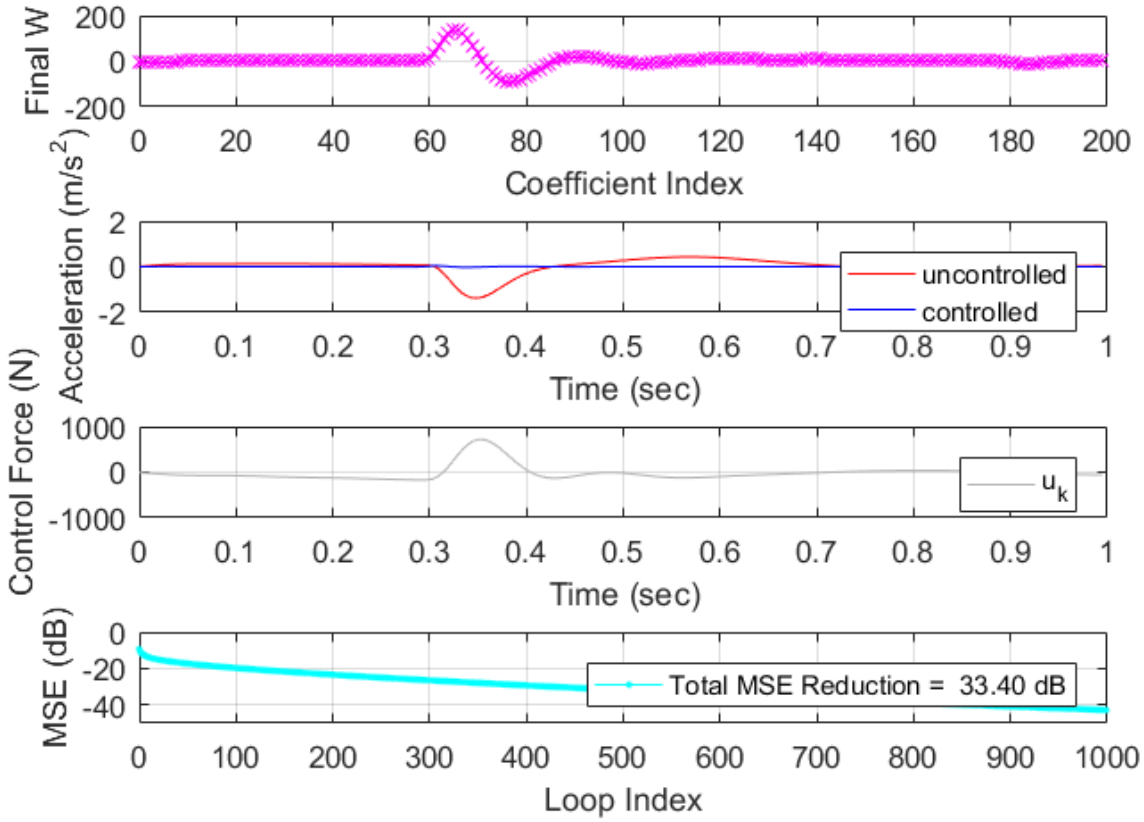

Figure 5.6: Sample iterative Fx-LMS adaptation with higher gain constant

The figures 5.5 and 5.6 show the adaptation process for lower and higher gain constants. All other conditions remained the same in the simulation. It can be seen that the reduction in mean square error is 33.40 dB with a higher gain constant compared to 15.55 dB with a lower gain constant. Thus, the choice of gain constant controls the rate of convergence of the adaptive filter.

The number of iterations and the gain constant are parameters that are chosen by trial and error. They must be chosen such that the filter remains stable and the convergence happens efficiently depending on the needs. This study is offline and hence the rate of convergence is of lower importance than stability. Thus, lower step sizes and higher number of iterations can be chosen without time constraints.

5.2 Fx-LMS application to the Plant

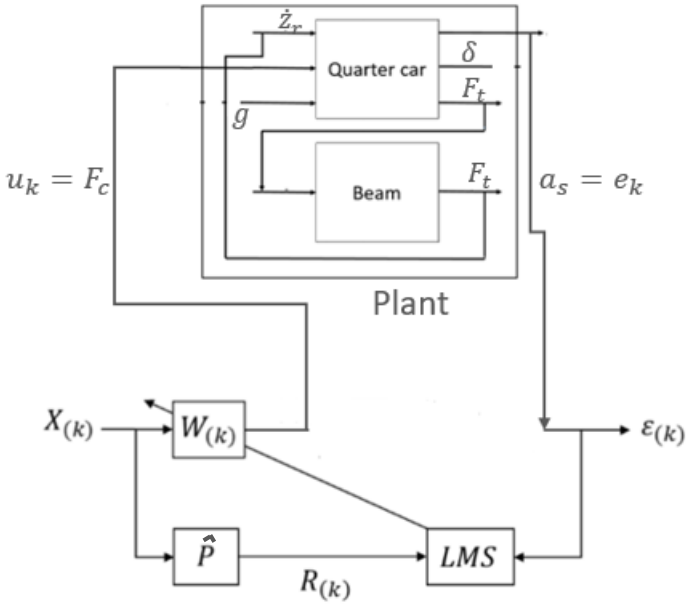

Figure 5.7: Fx-LMS applied to the plant in this study

Figure 5.7 represents the filtered-X-LMS applied to the plant that is used in this study, which is a quarter car model on a compliant surface. The main input to the system is the control force, F_c which is represented as u_k in figure 5.3. The major output which needs to be controlled is the acceleration of the sprung mass, a_s which is represented as ε_k in figure 5.3. This is the error signal. The error signal is the difference between the desired signal and the actual output signal. In this plant, the error signal need not be calculated and is an inherent output of the plant, as it is the response that is to be controlled. $\hat{P}$ is an estimate of the plant model. The adaptive filter requires an estimate of the plant model. The frequency response functions of the different plant models help decide the plant estimate to be used.

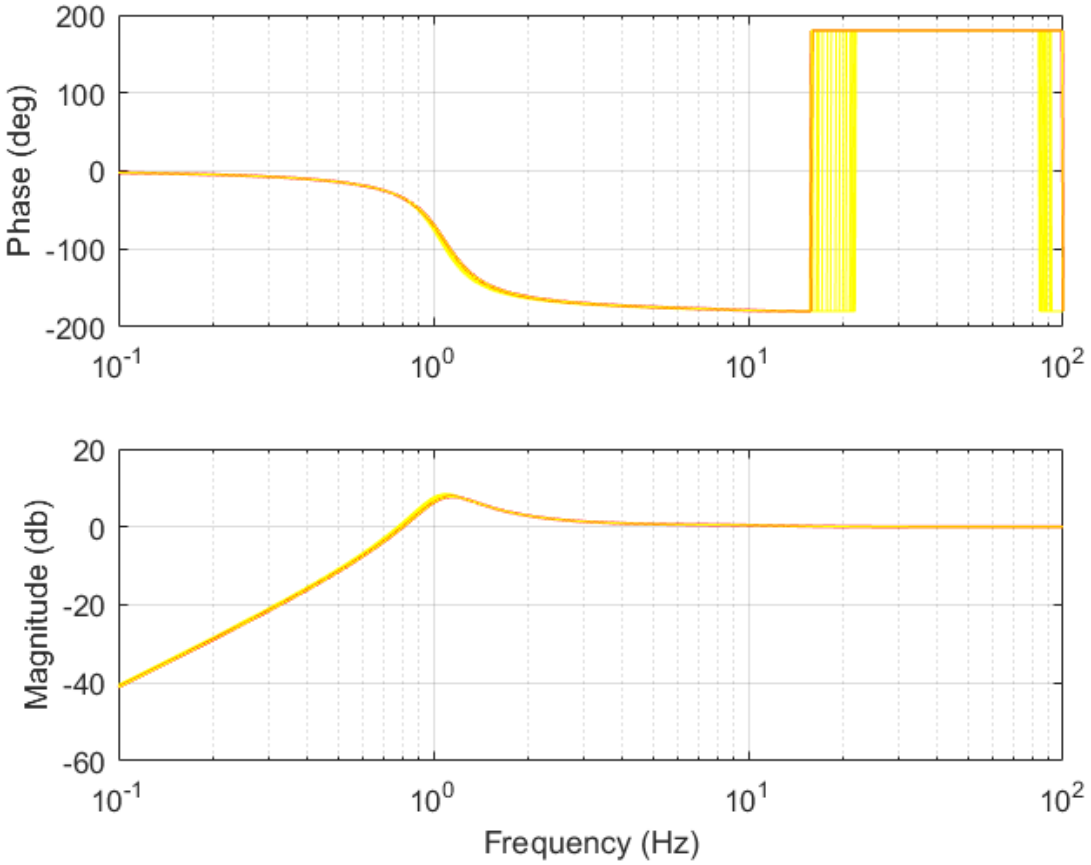

Figure 5.8: Frequency responses of all plant models as vehicle moves on foundation

The frequency response functions of all the different models as the vehicle moves on the foundation have been shown in figure 5.8. The input here is the control force and the output is the sprung mass acceleration. From the frequency responses shown in figure 5.8, we can see that the magnitude and phase of all the models are very similar. This is because the parameters have been chosen such that the impedance of the road is greater than the impedance of the suspension system. Since the frequency response functions are so similar for all the models, a single model can be chosen as the plant estimate in the adaptive filter. The LTI model of the vehicle in the middle of the beam has been used as the plant estimate in this study.

The filtered-X-LMS is applied to this acceleration response and is represented by the "LMS" block. The equation used in this block is the same as equation 5.4. An iterative process is used to calculate the next set of weights that can minimize the error signal, which is the acceleration response in this case. It is assumed that the actuator has unlimited authority over the control force

it can be produced. Hence, this estimation method will use gradient descent method to mathematically arrive at control forces that will minimize the error signal or the acceleration response.

6 Results

6.1 Choice and effect of different reference signals

In figure 5.7, X_k is the reference signal that excites the dynamics of the adaptive filter. The choice of reference signal has an effect on the adaptation process. The reference signals were chosen such that they correlate with the response which is the acceleration in this study. The reference signal is very important since it gives the adaptive filter an estimate of the response as the vehicle moves on the foundation and this is required for the adaptive filter to function.

To choose a reference signal, four different reference signals were used to run the simulation for the adaptation process. The reference signal that performed the best was chosen for the final case study. In the reference signals that have been shown below, the black line represents the start of the compliant surface and it ends when the reference signal becomes zero.

6.1.1 Reference signal 1

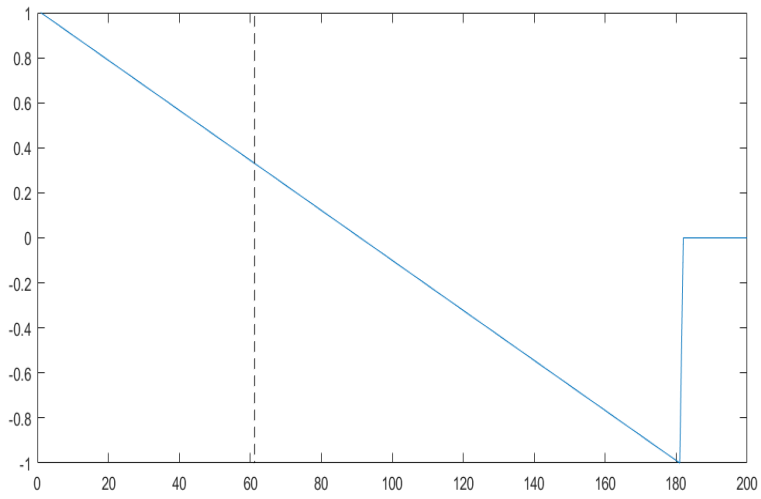

Figure 6.1: Reference signal 1

The figure 6.1 shows the first reference signal that was considered. For this reference signal, there was a total mean square error reduction was 7.61 dB.

6.1.2 Reference signal 2

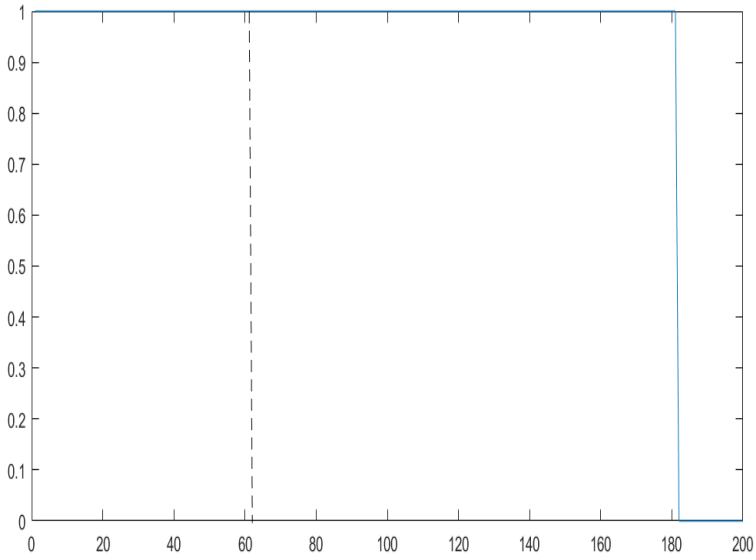

Figure 6.2: Reference signal 2

The figure 6.2 shows the next reference signal that was considered. The total mean square error reduction for this reference signal was 9.56 dB.

6.1.3 Reference Signal 3

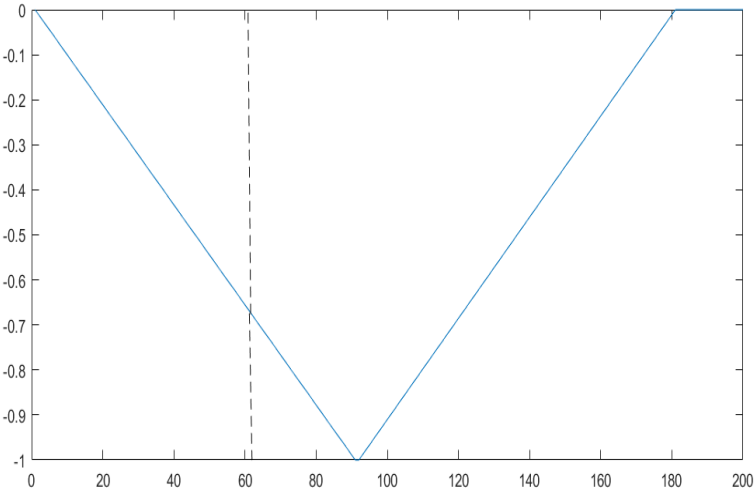

Figure 6.3: Reference signal 3

The figure 6.3 shows the next reference signal that was considered. The total mean square error reduction for this reference signal was 8.56 dB.

6.1.4 Reference Signal 4

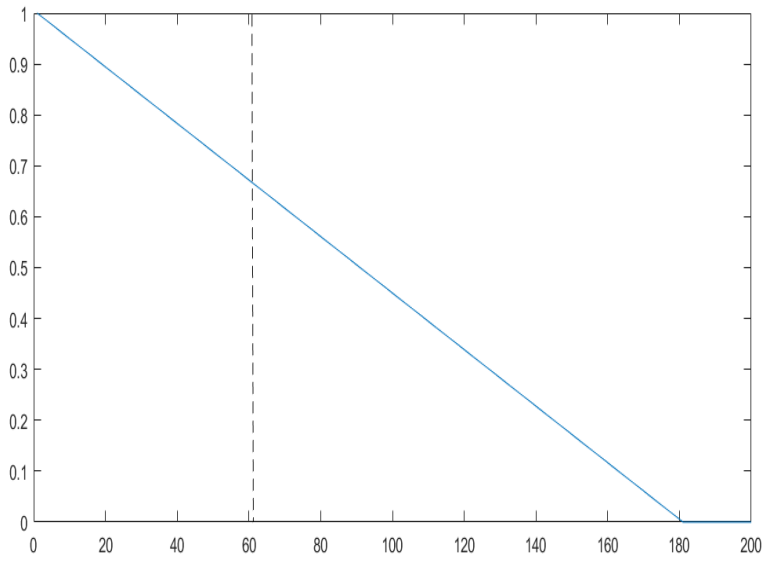

Figure 6.4: Reference signal 4

The figure 6.4 shows the final reference signal that was considered. The total reduction in mean square error is 12.94 dB for this reference signal.

Thus, from these results, it can clearly be seen that the choice of reference signal has a huge impact on the adaptation process. The choice of reference signals is hence important since it can make the adaptation process more efficient. Reference signal 4 leads to the highest reduction in total mean square error based on these results. This reference signal was used for the simulation of an Fx-LMS adaptation of a moving quarter car on a compliant surface.

6.2 Estimation of Ideal Control Force

The aim of this research is to estimate the ideal control force that is required to minimize the acceleration of the sprung mass while a vehicle travels on a compliant surface. To achieve this, the quarter car model was chosen as the model for the vehicle. The model for the compliant surface was developed. The two sub-models, the vehicle and the compliant surface were combined to obtain a plant. The plant was then simulated with a fixed set of parameters as a case study. The

control force to minimize this response was then estimated using filtered-X-LMS which has been described in the previous section. The parameters that were chosen for the quarter car and the beam have been given in tables 3.1 and 3.2. The only difference is the parameters for stiffness and damping coefficients of the foundation which have been shown in equation 4.1.

Two case studies were conducted for the car travelling at two different speeds. A low speed and high speed case were considered.

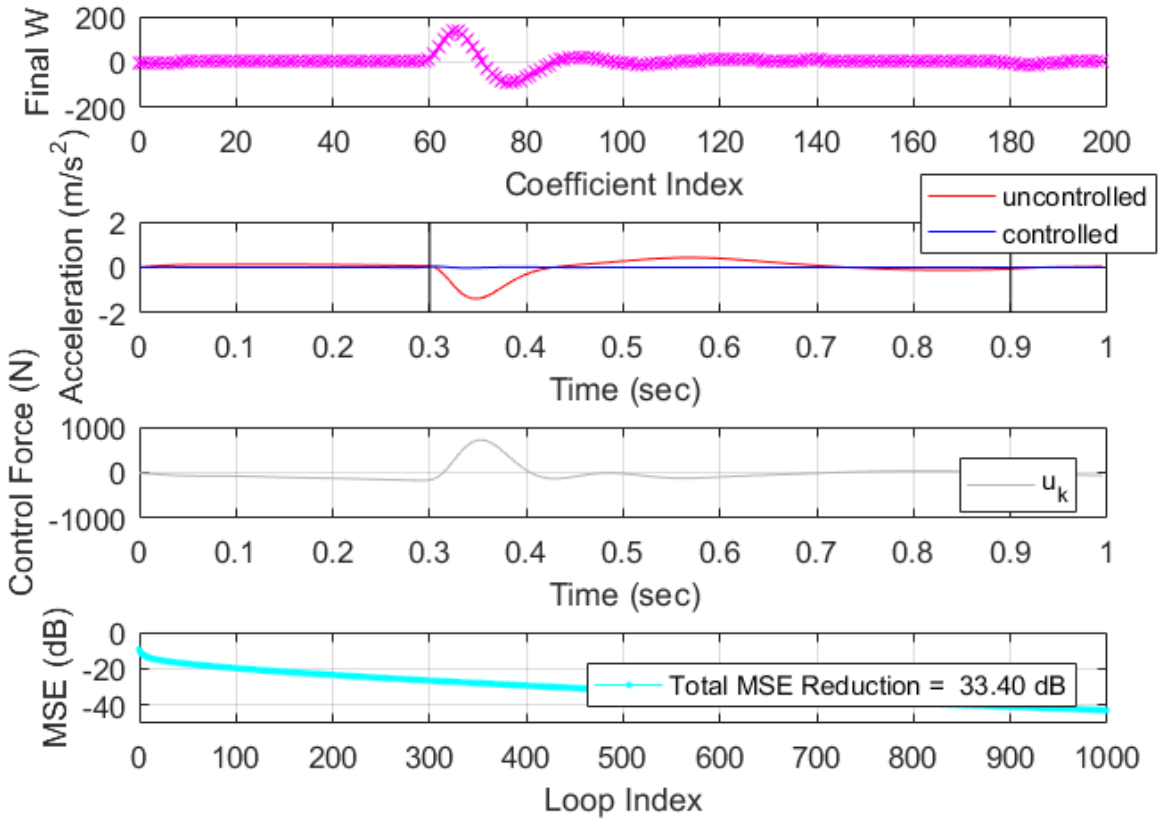

Figure 6.5: Fx-LMS adaptation for quarter car on compliant surface for low speed (10 mph)

The figure 6.5 shows the results of the adaptation for a moving quarter car on a compliant surface for a low speed case. The iterative LMS algorithm was tuned to run for 1000 iterations and the reduction of mean square error through the iterations can be seen. The total reduction in MSE was 33.40 dB. This is a very high drop in response and was achieved by efficiently tuning the LMS algorithm. The uncontrolled and controlled acceleration have been shown in the figure. The peak

uncontrolled acceleration was $-1.374\ m/s^2$. The peak controlled acceleration was $0.028\ m/s^2$. The adaptation process brought down the peak acceleration to almost zero. The first vertical black line represents the start of the compliant road and the second vertical line represents the end. Thus, the filter is allowed some time to start acting before the event is reached. The estimation of the peak control force was the major objective. This was obtained from the plot of control force versus time in figure 6.5. The peak control force was 717.4 N.

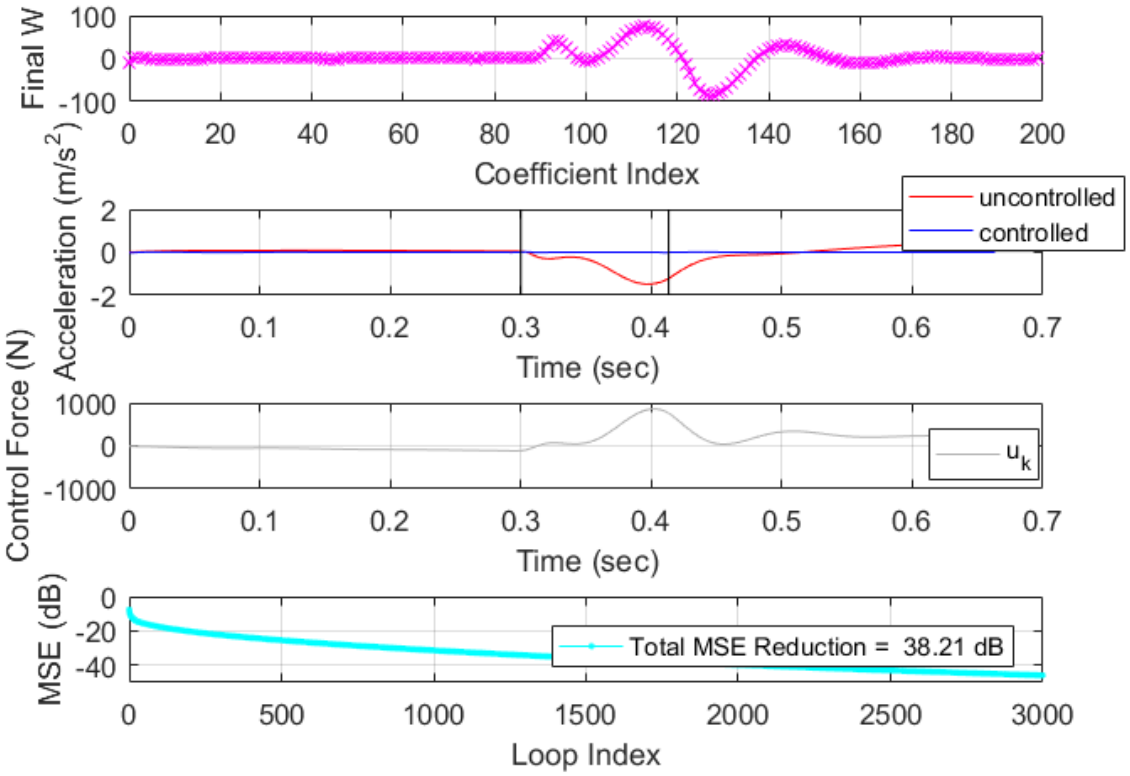

Figure 6.6: Fx-LMS adaptation for quarter car on compliant surface for high speed (60 mph)

The figure 6.6 shows the adaptation process for a quarter car moving on a compliant surface for a high speed case. The total reduction in mean square reduction is 38.21 dB. This was achieved with 3000 iterations. Thus, the process took three times more time than the low speed case. Another interesting observation was that there was a delay in achieving the peak acceleration in the high speed case.

From figure 6.6, we can see the uncontrolled and the controlled peak acceleration. The uncontrolled peak acceleration was 1.486 m/s^2 and the controlled peak acceleration was 0.0007 m/s^2. The peak control force that was estimated was 859.4 N. Similar to the first case study, the first black line represents the start of the compliant surface and the second black line represents the end of the compliant surface. Thus, the peak control forces were estimated for both cases. The final step would be to estimate the bandwidth.

6.3 Bandwidth

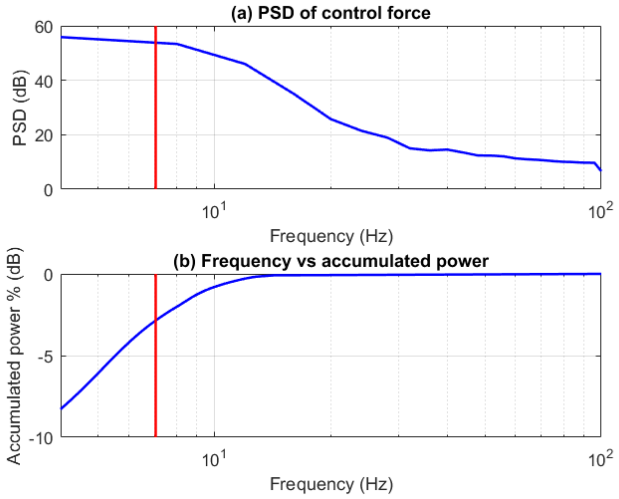

Figure 6.7: 80% Power Bandwidth for low speed case

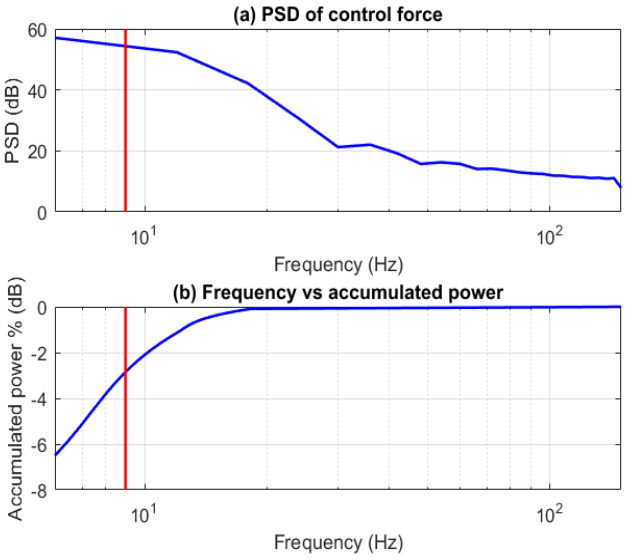

Figure 6.8: 80% Power Bandwidth for high speed case

Figure 6.7 and 6.8 show the power spectral density of the control force for the high speed and low speed cases, respectively. The plot of fervency versus total power accumulated was used to find the frequency at which more than 80% of the power is present.

$$P = \left\{ f(J): \frac{\sum_{i=1}^{J} PSD(i)}{\sum_{i=1}^{N} PSD(i)} = 0.8; J \in N \right\} \tag{6.1}$$

Equation 6.1 represents the 80% power bandwidth. $f(J)$ is the frequency at bin J and N is the total number of frequency bins for the PSD.

We can see from figure 6.7, that the for the chosen input, more than 80% of the total accumulated power is below 7 Hz which is represented by the vertical red line. Similarly, in figure 6.8, more than 80% of the total accumulated power is below 9 Hz which is represented by the vertical red line

7 Conclusion

A coupled dynamic system was developed for studying the dynamic interaction between a compliant road surface and a quarter-car model with an active suspension element. This coupled system enabled the development of a method for estimating the ideal force profile to substantially cancel sprung mass acceleration.

The Filtered-X LMS algorithm was modified to be able to generate an estimate of the ideal force profile for this coupled dynamic system. The primary modification involved a simplified model of the coupled plant dynamics in order to eliminate the need for a time-varying model.

A reference profile was developed that significantly improved the overall convergence of the estimation process. This reference profile was realistic in the sense that it did not require a priori information about the compliant road surface other than its spatial extent, which could easily be determined from a vision system.

The method was applied to a simulation case study of a quarter-car with an active suspension moving at a constant velocity across a compliant boundary condition. This simulation also included starting and ending on a non-compliant boundary condition. The results from this case study demonstrate that an ideal force profile can be obtained such that the actively controlled sprung mass acceleration is virtually zero. These results also enable the extraction of key active system design parameters such as peak force and actuator bandwidth.

Since the estimation of peak control force and bandwidth are two of the key factors in the design of actuators in suspension systems [4, 5, 6], this work would be a major contribution.

7.1 Future Work

This work was limited to a quarter car model. This can be extended to a full-vehicle model with higher degree of freedoms. This will allow for additional forces from pitch and roll, thereby making the model more realistic.

Currently, this work does not claim to be able to understand the interactions within the compliant surface, for example, interactions in soft soil which may lead to other ways of modeling. The current scope of this work is limited since the soil parameters are lumped up into stiffness and

damping as a function of position on the compliant surface. Research into soil modeling and terra-mechanics may help expand the current scope of the model.

The results of this simulation could be used to create actuators. Also, testing methodologies can be developed to practically test the operation of a quarter car on a compliant surface and implement a controller based on the results of this study.

8 References

1. Sharp, R.S. and D.A. Crolla, *Road Vehicle Suspension System Design - a review.* Vehicle System Dynamics, 1987. **16**(3): p. 167-192.
2. Tseng, H.E. and D. Hrovat, *State of the art survey: active and semi-active suspension control.* Vehicle System Dynamics, 2015. **53**(7): p. 1034-1062.
3. Rao, A. M. (2016). *A Structured Approach to Defining Active Suspension Requirements* (Master's Thesis, Virginia Tech).
4. Gysen, B.L., et al., *Active electromagnetic suspension system for improved vehicle dynamics.* IEEE Transactions on Vehicular Technology, 2010. **59**(3): p. 1156-1163.
5. Weeks, D., et al., *The design of an electromagnetic linear actuator for an active suspension*. 1999, SAE Technical Paper.
6. Iijima, T., et al., *Development of a hydraulic active suspension*. 1993, SAE Technical Paper.
7. Ghazaly, N.M. and A.O. Moaaz, *The Future Development and Analysis of Vehicle Active Suspension System.* IOSR Journal of Mechanical and Civil Engineering, 2014. **11**(5): p. 19-25.
8. Thompson, A., *An active suspension with optimal linear state feedback.* Vehicle system dynamics, 1976. **5**(4): p. 187-203.
9. Ting, C.-S., T.-H.S. Li, and F.-C. Kung, *Design of fuzzy controller for active suspension system.* Mechatronics, 1995. **5**(4): p. 365-383.
10. Nguyen, T.T., et al. *A hybrid control of active suspension system using H∞ and nonlinear adaptive controls*. in *Industrial Electronics, 2001. Proceedings. ISIE 2001. IEEE International Symposium on*. 2001. IEEE.
11. Bender, E.K., *Optimum Linear Preview Control With Application to Vehicle Suspension.* Journal of Basic Engineering, 1968. **90**(2): p. 213-221.
12. Tomizuka, M., *"Optimum Linear Preview Control With Application to Vehicle Suspension"—Revisited.* Journal of Dynamic Systems, Measurement, and Control, 1976. **98**(3): p. 309-315.
13. Louam, N., D. Wilson, and R. Sharp, *Optimal control of a vehicle suspension incorporating the time delay between front and rear wheel inputs.* Vehicle system dynamics, 1988. **17**(6): p. 317-336.
14. Adibi Asl, H. and G. Rideout. *Using lead vehicle response to generate preview functions for active suspension of convoy vehicles*. in *American Control Conference (ACC), 2010*. 2010.
15. Hać, A., *Optimal linear preview control of active vehicle suspension.* Vehicle system dynamics, 1992. **21**(1): p. 167-195.
16. E. Winkler, Die Lehre von der Elastizitat und Festigkeit, Dominicus, Prague, 1867.
17. Dutta, Sekhar Chandra, and Rana Roy. "A critical review on idealization and modeling for interaction among soil–foundation–structure system." *Computers & structures* 80.20 (2002): 1579-1594.
18. Bernard Widrow, S.D.S., *Adaptive Signal Processing*. 1985: Prentice Hall. 475.
19. Song, X., et al., *An Adaptive Semiactive Control Algorithm for Magnetorheological Suspension Systems.* Journal of Vibration and Acoustics, 2005. **127**(5): p. 493-502.